Mechanical properties of graphene nanoribbons

2009 J. Phys.: Condens. Matter 21 285304

(http://iopscience.iop.org/0953-8984/21/28/285304)

J. Phys.: Condens. Matter **21** (2009) 285304 (7pp) doi:10.1088/0953-8984/21/28/285304

Mechanical properties of graphene nanoribbons

Ricardo Faccio[1,2,4], Pablo A Denis[3], Helena Pardo[1,2], Cecilia Goyenola[1,2] and Álvaro W Mombrú[1,2]

[1] Crystallography, Solid State and Materials Laboratory (Cryssmat-Lab), DETEMA, Facultad de Química, Universidad de la República, Avenida General Flores 2124, PO Box 1157, Montevideo, Uruguay
[2] Centro NanoMat, Polo Tecnológico de Pando, Facultad de Química, Universidad de la República, Camino Aparicio Saravia s/n, 91000, Pando, Canelones, Uruguay
[3] Computational Nanotechnology, DETEMA, Facultad de Química, Universidad de la República, Avenida General Flores 2124, CC 1157, 11800 Montevideo, Uruguay

E-mail: rfaccio@fq.edu.uy

Received 24 February 2009, in final form 21 May 2009
Published 19 June 2009
Online at stacks.iop.org/JPhysCM/21/285304

Abstract
Herein, we investigate the structural, electronic and mechanical properties of zigzag graphene nanoribbons in the presence of stress by applying density functional theory within the GGA-PBE (generalized gradient approximation-Perdew–Burke–Ernzerhof) approximation. The uniaxial stress is applied along the periodic direction, allowing a unitary deformation in the range of ±0.02%. The mechanical properties show a linear response within that range while a nonlinear dependence is found for higher strain. The most relevant results indicate that Young's modulus is considerable higher than those determined for graphene and carbon nanotubes. The geometrical reconstruction of the C–C bonds at the edges hardens the nanostructure. The features of the electronic structure are not sensitive to strain in this linear elastic regime, suggesting the potential for using carbon nanostructures in nano-electronic devices in the near future.

(Some figures in this article are in colour only in the electronic version)

1. Introduction

Recently a new carbon nanostructure, called the graphene nanoribbon (GNR), has emerged and attracted the attention of the scientific community because of the promise for its use in spintronics. It is mainly attributed to the work of Son *et al* [1, 2], who predicted that an in-plane electric field, perpendicular to the periodic axis, induces a half-metal state in zigzag nanoribbons (ZGNR). Apart from the interesting dependence of the electronic structure upon an electric field, this is a promising material for future spintronic devices, since it could work as a perfect spin filter. Very recently Campos-Delgado *et al* [3] reported a chemical vapour deposition route (CVD) for the bulk production of long, thin, and highly crystalline graphene ribbons (less than 20–30 μm in length), with widths from 20 to 300 nm and small thicknesses (2–40 layers). This experimental advance further increases the expectations for the use of these materials in high-tech devices.

In parallel there is increased interest in the physical properties of carbon nanostructures in general, due to their outstanding mechanical and electronic properties. Recently, Lee *et al* [4] measured the mechanical properties of a single graphene layer, demonstrating that graphene is the hardest material known, since its elastic modulus reaches a value of 1.0 TPa. In addition, much effort has been dedicated to studying the electronic properties of graphene, because creating a gap could allow the use of graphene in field effect transistors. Many mechanisms have been proposed for that purpose: nano-patterning, creating quantum dots, using multilayers, covalent functionalization [5], doping with heteroatoms such as sulfur [6] and applying mechanical stress [7, 8]. In this last case, within linear elasticity theory and a tight-binding approach, Pereira *et al* [8] observed that strain can generate a bulk spectral gap. However this gap is critical, requiring threshold deformations in excess of 20%, and only along preferred directions with respect to the underlying lattice.

[4] Author to whom any correspondence should be addressed.

The evidence presented above clearly indicates that it is important to know how the electronic properties of ZGNR depend on stress, in order to predict its performance in future devices (e.g. gates).

In the literature, many representative results concerning the simulation mechanical properties of carbon nanostructures can be found. In particular classical methods have been widely and successfully applied to: polymerized nanotubes [9], nanotube networks [10], 'super' carbon nanotubes [11] and Möbius and twisted graphene nanoribbons [12]. However there are very few reports relating to the study of strain in graphene nanoribbons [13–15] and none of them report Young's modulus. The main conclusions from these works indicate that there is no important variation of the electronic properties of zigzag nanoribbons due to stress–strain effects (i.e. energy gaps and local magnetic moments) and there is no information regarding the mechanical properties of this nanostructure.

To the best of our knowledge, in this work we present the first systematic determination of Young's modulus, Poisson's ratio and the calculated shear modulus for graphene nanoribbons. The paper is structured as follows. In section 1.1 we describe the state of the art regarding the mechanical properties of carbon nanoribbons and related nanostructures. In section 1.2 we briefly review the most relevant features of the electronic structure of ZGNR for the present simulation. In section 3, we present and discuss Young's modulus, Poisson's ratio and the shear stress for different ZGNR.

1.1. Mechanical properties of carbon nanostructures

Young's modulus 'E' is a measure of the stiffness of a solid, and together with two additional elastic parameters (the shear modulus 'G' and Poisson's ratio 'υ') defines the mechanical properties of the material. In the case of graphene, because of the reduced dimensionality, it makes more sense to define the in-plane stiffness (E^{2D}) rather than the classical 3D Young's modulus (E^{3D}). For this reason in graphite the elastic properties can be considered independent of the interlayer distance between graphene, $c_0 = 3.35$ Å, and Young's modulus can be described as follows: $E^{2D} = \frac{1}{A_0}(\frac{\partial^2 E_S}{\partial \varepsilon_x^2})_{E_0} = E^{3D}c_0$, where E_S, ε_x and A_0 corresponds to the total energy, linear strain and equilibrium reference area of the 2D material, respectively. The in-plane stiffness of graphite is obtained by considering an axial load over graphene. The value obtained in this case is $E^{3D} = 1.02(3)$ TPa [16]. It allows us to obtain $E^{2D} = 3.41(9)$ TPa Å. This value is almost identical to that obtained experimentally for graphene, $E^{2D} = 3.42(30)$ TPa Å [4], using nano-indentation with an atomic force microscope. This result is in agreement with those reported by Kudin *et al* [17] and Van Lier *et al* [18]. Using *ab initio* methods they reported a Young's modulus of $E^{3D} = 1.02$ TPa Å [17] and 1.11 TPa Å [18]. Poisson's ratio is unambiguously defined in terms of the transverse ratio over the longitudinal variation, and has a value of $\upsilon = 0.149$. Many representative results for graphene and nanotubes, based on Reddy *et al* [19] and other workers, are presented in table 1 [10, 17–30].

Table 1. Representative results for different carbon nanostructures.

Reference	E^{3D} (TPa)	υ	Remarks
	Graphene		
[10]	0.799	—	Graphene (force field)
[17]	1.02	0.149	Graphene (*ab initio*)
[18]	1.11	—	Graphene (*ab initio*)
[19]	1.012	0.245	Graphene (Brenner[a])
[19]	0.669	0.416	Graphene (Brenner[b])
[20]	0.694	0.412	Graphene (Brenner)
[24]	1.11	0.45	Graphene (truss model)
Present work	0.96	0.17	Graphene (*ab initio*)
	Carbon nanotubes		
[21]	0.694	—	SWNT (Brenner)
[23]	0.97	0.28	SWNT (empirical model)
[25]	0.213–2.08	0.16	SWNT (MM)
[26]	0.32–1.47	—	SWNT (experiments)
[27]	0.7	—	SWNT (MD)
[28]	1.0	0.25	DWNT (vibrations)
[29]	0.81–1.13	—	SWNT (experiments)
[30] [c]	0.8–1.05	—	SWNTS (*ab initio*)
[30]	1.05	—	SWNT (5, 5)-(*ab initio*)
Present work	1.01	—	SWNT (5, 5)-(*ab initio*)

[a] Non-minimized potential; [b] minimized potential; [c] this result was converted to E^{3D} for comparison purposes, using: $E^{3D} = E^{2D}c_0$.

Single-walled carbon nanotubes (SWCNT) are an example of a one-dimensional system described in terms of a 2D property E^{2D}, since two parameters must be given, the tube length (L) and the tube radius (r), in order to gain independence from size effects. Several expressions have been published for their mechanical properties in terms of multidimensional Young's moduli: E^{3D}, E^{2D}, etc. [29, 30]. The values reported show a wide variation in experimental E^{nD} values, with up to an order of magnitude of difference. This is mainly due to the difficulty in determining the precise structure of the nanotubes under study, the presence of defects, chirality, etc. Recently, Wu *et al* [29] used the combined optical characterization of individual SWCNT, coupled with an magnetic actuation technique, to measure Young's modulus of nanotubes with a known chirality. Young's modulus was $E^{3D} = 0.97(16)$ TPa, assuming a wall thickness of $c = 3.4$ Å corresponding to the interlayer spacing in graphite. Within the experimental accuracy no dependence on the nanotube's chiral index was found. This result agrees quite well with theory, in particular with the values reported by Bogár *et al* [30]. Employing an all electron DFT method, they reported E^{2D} for different tube radii ranging from $r = 1.32$ to 4.11 Å. They concluded that there is no dependence between Young's modulus and the chirality of the nanotube.

1.2. Electronic and geometrical structure of zigzag nanoribbons

In graphene nanoribbons, the presence of different types of boundary shapes, called edges, modifies the electronic structure of the material. The major effects are observed at the Fermi level, displaying unusual magnetic and transport

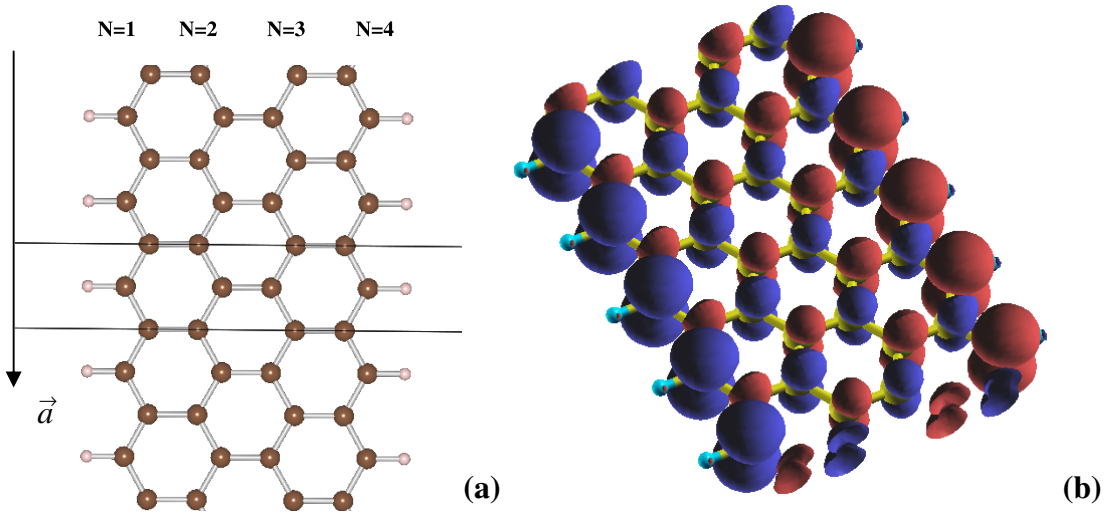

Figure 1. (a) Graphene nanoribbon with $N = 4$, displaying its smallest unit cell; the arrow shows the periodic direction $\vec{a}$. (b) Spin density map, showing the antiferromagnetic arrangement between opposite edges.

Table 2. Energy gaps for different zigzag graphene nanoribbons.

Width (N)	Energy gap (eV)
4	0.63
5	0.59
6	0.54
7	0.50
8	0.46
9	0.43
10	0.40

features [31]. The zigzag edges present electronic localized states at the boundaries, corresponding to non-bonding states that appear at the Fermi level as a large peak in the density of states. The non-magnetic solution has many states at the Fermi level, which produce a strong instability that can be resolved by spin polarization or geometrical distortion. Due to the non-bonding character of the zigzag localized edge states, the geometrical reconstruction is unlikely to happen [32] and the spin polarization of the electronic density establishes an antiferromagnetic arrangement with the opening of a gap, yielding a Slater insulator [33]. The opening of the gap is related to the ZGNR width, since it is a consequence of the interaction between edges. For this reason wider ribbons, with longer distances between opposite edges, recover the graphene geometry with a gap equal to zero. The tendency observed corresponds to an exponential decay of the energy gap when increasing the nanoribbon width (N). Table 2 shows our results for $N = 4, 5, 6, 7, 8, 9$ and 10 (see figure 1).

2. Methods

The theoretical study of the uniaxial stress on different ZGNR is based on first principles density functional theory [34, 35], which we successfully used to study, bulk graphene, thioepoxidated SWCNT, sulfur doped graphene and double wall CNT [6, 36–38]. The simulations are performed using the SIESTA code [39–41], which adopts a linear combination of numerical localized atomic-orbital basis sets for the description of valence electrons and norm-conserving non-local pseudopotentials for the atomic core. The pseudopotentials were constructed using the Troullier and Martins scheme [42], which describes the interaction between the valence electrons and atomic core. We selected a split-valence double-ζ basis set with polarization orbitals for all the carbon atoms. The extension of the orbitals is determined by cutoff radii of 4.994 and 6.254 au for the s and p channels respectively, as obtained from an energy shift of 50 meV due to localization. The total energy was calculated within the Perdew–Burke–Ernzerhof (PBE) form of the generalized gradient approximation (GGA) xc-potential [43]. The real-space grid used to represent the charge density and wavefunctions was the equivalent of that obtained from a plane-wave cutoff of 230 Ryd. The atomic positions were fully relaxed in all cases by using a conjugate gradient algorithm [44] until all forces were reduced to less than 10 meV Å^{-1}. A Monkhorst–Pack grid [45] with a $300 \times 2 \times 2$ supercell, defined in terms of the actual supercell, was selected to obtain a mesh of 600 k-points in the full Brillouin zone. All these parameters allow the convergence of the total energy, which corresponds to the antiferromagnetic solution in all cases.

In order to validate our methodology we calculated Young's modulus of (5, 5) SWCNT, for which the literature shows several results from *ab initio* methods (see table 1). The smallest unit cell contains a total of 20 carbon atoms. With the purpose of studying the dependence on the number of carbon atoms, we simulated the case of 40 carbon atoms per unit cell. The Young's moduli obtained are $E^{3D} = 1.03(2)$ and $E^{3D} = 1.01(3)$ TPa, respectively, for 20 and 40 carbon atoms in the unit cell. The results are consistent within the uncertainty, which was estimated from the variance obtained from the adjustment of the second order fitting of the energy upon unitary deformation. Therefore one can conclude that the

results are not affected by the number of supercells used along the periodic direction.

Additionally the results are in good agreement with those reported in the bibliography; see table 1, particularly the excellent agreement with those from Bogár *et al* [30]. However there exist some differences in Young's modulus of graphene obtained by classical methods. Force field approaches seem to underestimate Young's modulus of graphene by 20% [10]. In the case of Brenner potentials, it has been demonstrated there is a strong dependence of E^{3D} on the equilibrium adjustment yield used in the calculation [19]. Young's modulus changes from 1.11 to 0.7 TPa when the potential is optimized. For this reason any comparison should be done taking into account the methodology involved in the simulation.

Regarding the geometry in graphene nanoribbons, we can distinguish two C–C bond orientations: the bond perpendicular to the crystalline periodic direction $d(|)$ and the bond diagonal to the normal direction $d(/)$. The bond distances differ from the inner part of the ribbon (bulk) with respect to the atoms at the edge. In the case of bulk C–C distances we found $d(|)_{\text{bulk}} = 1.44$ Å and $d(/)_{\text{bulk}} = 1.44$ Å, while at the edge of the ribbon we found $d(|)_{\text{edge}} = 1.46$ Å and $d(/)_{\text{edge}} = 1.43$ Å. This result agrees with the tendency observed by Pisani *et al* [33], where the perpendicular bond elongates at the edge, contracting the corresponding diagonal bond at the edge. It promotes an increase of the zigzag C–C–C angle from 120° in the bulk to 121.9° at the edge. This trend is observed for the whole unstressed studied ribbons.

For all of these reasons, we can unequivocally conclude that our methodology is valid.

The ZGNR selected for the simulation correspond to $N = 4, 5, 6, 7, 8, 9$ and 10. Since the code applied was designed for three-dimensional materials, we designed special unit cells. All the cells were orthogonal, with the GNR placed in the *ab* plane, and oriented with the periodic direction along the *a* axis, see figure 1 for the ZGNR $N = 4$ sketch. In order to avoid interference between symmetry images, vacuum regions of 15 Å were added along the *b* and *c* directions. In the case of the smallest unit cell, the *a* axis value for every cell is approximately $a_0 = 2.495$ Å, with a total number of atoms of $2N + 2$. With the purpose of increasing the number of degrees of freedom in each case, the cells were expanded in units of four along the *a* axis ($a = 4a_0$), it allows us to multiply by four the number of atoms inside the supercells, according to $8N + 8$. The total number of atoms in each case is: 40, 48, 56, 64, 72, 80 and 88.

3. Results and discussion

The stress–strain curves are obtained by applying varying stress to the GNR, then allowing full atomic relaxation together with full unit cell parameter optimization until the desired stress tensor is reached. Since we are considering only a uniaxial strain, the Voigt tensor has only one non-zero component: $[\sigma_x, \sigma_y, \sigma_z, \sigma_{xy}, \sigma_{xz}, \sigma_{yz}] \Rightarrow [\sigma_x, 0, 0, 0, 0, 0]$. The selected stress components of the Voigt tensor allow us to establish strains in the range of $\varepsilon_x = \pm 0.020$ for the whole series, which assures a linear stress regime [46, 47]. It

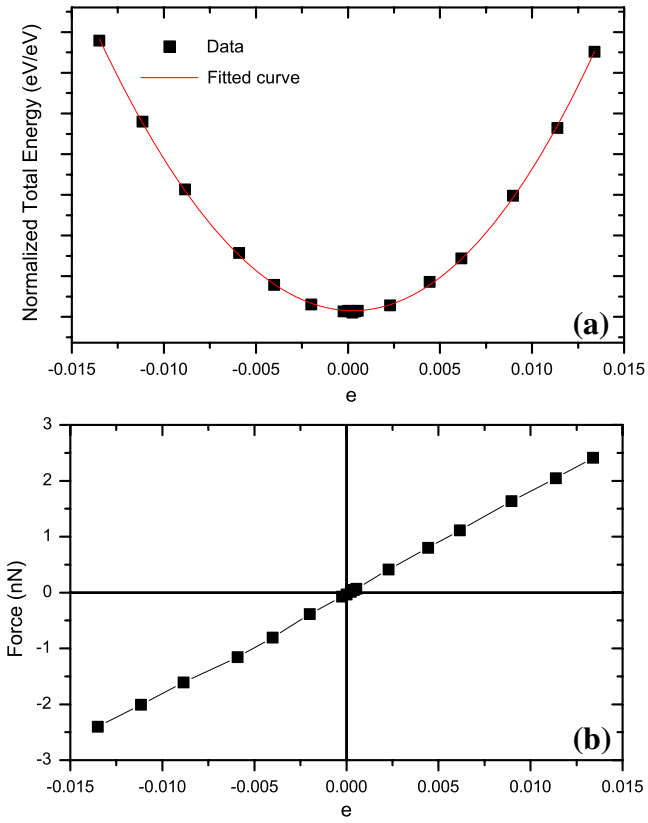

Figure 2. (a) Normalized total energy versus strain, and (b) the corresponding force versus strain for the ZGNR with $N = 10$, indicating a linear stress–strain regime.

corresponds to a quadratic dependence of the total energy upon the strain. The most important features of the data treatment are presented in figure 2 for the ZGNR where $N = 10$.

While the second derivative of the total energy is easily obtained, the reference surface is ambiguously defined, with a dependence of the results upon the surface selection. In particular, a problem arises with the selection of the GNR's width, since it is a surface of pruned edges. In our case we have selected two different ways of determining the reference width of the GNR: the shortest C–C width (d_A) and the longest C–C width (d_B). A sketch of these distances is presented in figure 3(a). It is clear that neither of them are the best selection, and this becomes a problem when we want to compare these results in the N-infinity limit, corresponding to graphene. For this reason all the results are presented, together with the results for graphene. Figure 3(b) shows the variation of E^{2D} with the GNR's width N. The same results are presented in table 3. To check the reliability of the calculations, the case of $N = \infty$ (graphene) was studied. In this case we take a rectangular supercell with 32 carbon atoms. Each periodic crystalline axis was oriented along the zigzag and armchair directions, selecting a c value of 20 Å in order to avoid interference between the images. The stress was applied along the zigzag axis. The obtained Young's modulus, $E^{3D} = E^{2D}/c_0 = 0.964(9)$ TPa, agrees quite well with earlier reported values (see table 1), and Poisson's ratio, $\upsilon = 0.17$, matches the ones reported by Kudin *et al* [17] ($\upsilon = 0.149$) and

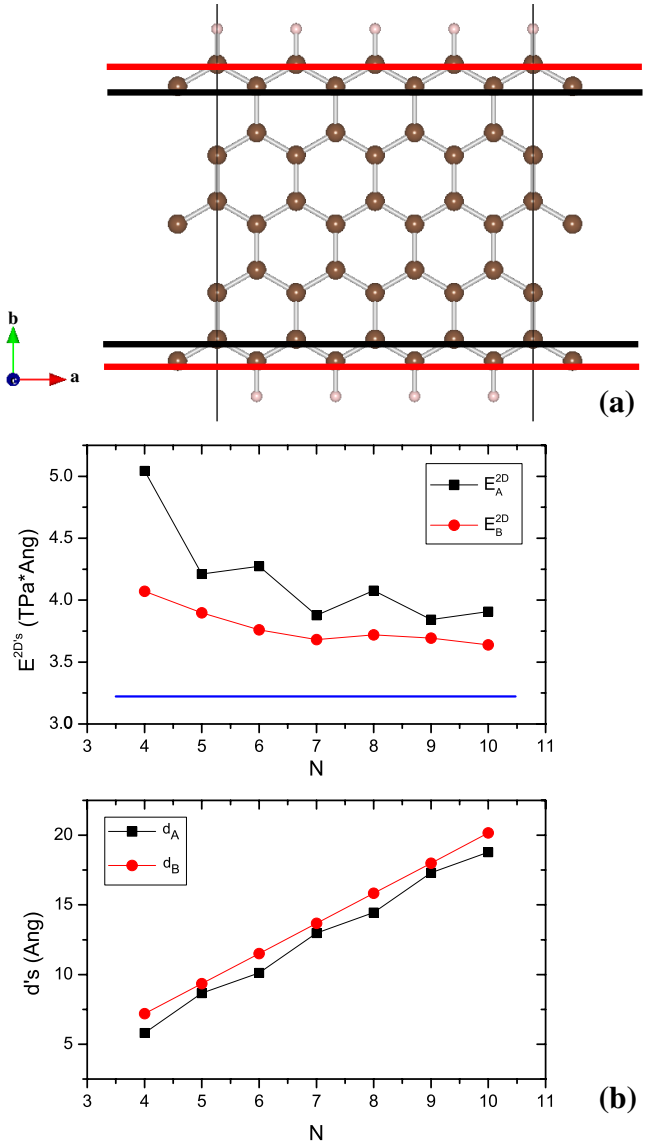

Figure 3. (a) The $N = 5$ ZGNR sketching the distances: d_A (square-black) and d_B (circle-red). (b) The E^{2D} Young's modulus according to the different distances considered in the model which are expressed in terms of the ribbon's width (N) in (c). The horizontal blue line corresponds to the graphene results. (Colour online.)

Liu *et al* [48] ($\upsilon = 0.186$). This is further evidence that helps us to validate our methodology.

It is important to note that the results with the greatest difference correspond to $E^{3D} = 0.799$ TPa. The universal force field seems to overestimate the bulk modulus and to underestimate the basal plane Young's modulus by 20%, in the case of perfect crystalline structures.

The results show E_A^{2D} and E_B^{2D} decrease when N increases, always having a Young's modulus higher than in graphene. We can argue that ZGNR are harder than graphene. This tendency is the opposite of the case for carbon nanotubes, and the reason can be easily explained in terms of graphene bending. The curvature of the CNT softens the rolled-up graphene sheet because of the loss of overlapping between

Table 3. Final E^{2D} Young's modulus obtained from the different GNR widths (d_i).

N	d_A	d_B (Å)	E_A^{2D} (TPa Å)	E_B^{2D}
4	05.80	07.19	5.04	4.07
5	08.66	09.35	4.21	3.90
6	10.12	11.51	4.27	3.76
7	12.98	13.68	3.88	3.68
8	14.45	15.83	4.08	3.72
9	17.30	18.00	3.84	3.69
10	18.77	20.16	3.91	3.64
∞	—		3.23	

Table 4. Poisson's ratio and estimated shear modulus for d_A and d_B models.

N	υ_A	υ_B	G_A	G_B
4	0.129	0.261	0.667	0.482
5	0.204	0.250	0.522	0.466
6	0.150	0.230	0.555	0.456
7	0.207	0.223	0.480	0.449
8	0.156	0.216	0.526	0.457
9	0.200	0.226	0.478	0.450
10	0.190	0.216	0.490	0.447
∞	0.179		0.408	

the sp^2 orbitals, with a more pronounced effect for smaller tubes [30]. In the case of GNR the sheet is always plane, with a perfect sp^2 overlapping and strong stiffness. In principle, this result should not be expected, but the response could be understood qualitatively in terms of two opposing effects: the curvature of graphene and geometrical edge reconstruction. The higher the curvature the lower the orbital overlap, and hence the lower the hardness. Furthermore our results indicate that the energy necessary to deform the ribbons (strain energy), expressed as energy per atom, is lower when more carbon atoms are involved; thus fewer atoms harden the material. The origin of this effect lies in the geometrical reconstruction of the C–C bonds positioned at the edge. As was mentioned in the introduction, the diagonal C–C distances of GNR at the edges contract by ∼0.02 Å, while at the same time the zigzag C–C–C angle increases by ∼2°, aligning the stronger C–C diagonal bonds more parallel to the periodic direction of the nanostructure and hardening the bonds. This effect is more evident in the case of thin GNR since there are few C–C bulk bonds, and as the GNR width increases, the bulk bonds prevail, diluting the effect of the harder C–C bonds at the edge. In the case of nanotubes the relaxation effect on the edge does not exist, and therefore the curvature effect prevails.

Poisson's ratio presents a similar tendency to the one observed for Young's modulus. The results are shown in figure 4 and table 4, where the $\upsilon_i = -\varepsilon_y^i/\varepsilon_x$ ($i = A$ and B) values are presented together with the value for graphene. The tendency between υ and N corresponds to a damped oscillation in the case of υ_A, while the dependency is smoother for the case of υ_B. In the extrapolated limit to infinite widths the ratios υ_i are $\upsilon_A = 0.18$ and $\upsilon_B = 0.22$.

The shear modulus can be obtained using $G^{3D} = E^{3D}/2(1+\upsilon)$. For graphene we obtained $G^{3D} = 0.408$ TPa.

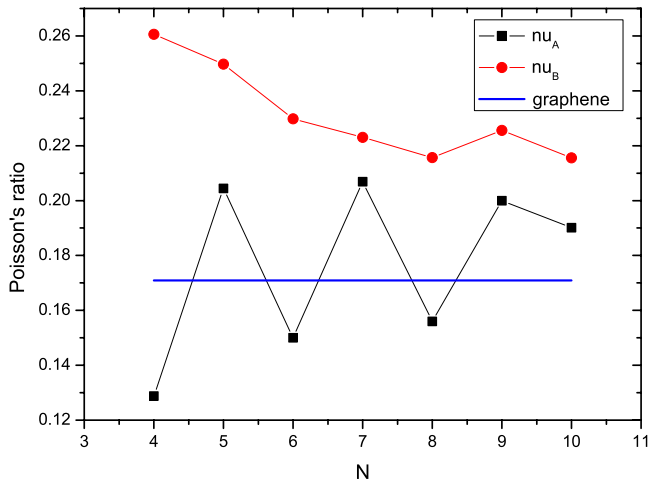

Figure 4. The υ dependence upon the GNR width (N). The horizontal blue line corresponds to the graphene results.

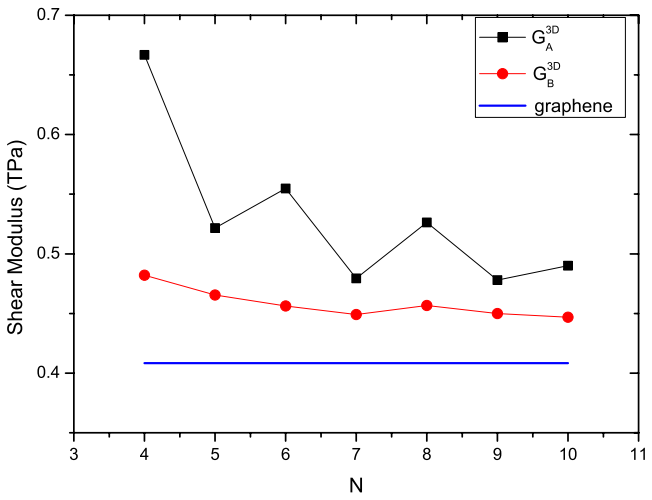

Figure 5. Shear modulus G^{3D} for GNR indicating the estimated value for graphene.

This value agrees with $G^{3D} = 0.384$ TPa reported by Reddy *et al* [19], but differs by a factor of almost two from those reported by Sakhaee-Pour [49]. Employing a force field method for finite graphene sheets, with different edge terminations, he obtained G values that ranged from 0.21 to 0.23 TPa. It is important to note that the corresponding Poisson's ratio reported by Sakhaee-Pour was calculated using E and υ. However our results are more similar to those reported for SWCNT [50, 51], for which there have been reported G^{3D} values ranging from 0.250 to 0.485 TPa. This is a valid reference for our results, since in this case the mechanical load involves only a single graphene layer. This is the main reason why the shear moduli of SWCNT are higher than MWCNT, since in this last case there exists a sliding effect between nanotubes that reduces the shear modulus. On the one hand, this discrepancy can be attributed to the different nature of the methods used for the simulation. On the other hand our results were estimated for two independent parameters E^{2D} and υ. Regarding the dependence of the shear modulus upon ribbon width, see figure 5 and table 4, we found a similar dependence to Young's modulus versus N. This is to be expected, since the shear modulus expression is dominated by its numerator, corresponding to Young's modulus, while the denominator remains almost constant, since Poisson's ratio remains almost constant. Further simulations, including shear deformation, should be done in order to shed more light on this subject.

Regarding the electronic structure features of GNR we found no significant dependence of these properties upon strain. These results agree with those reported earlier [13–15], whereas for the case of ZGNR a small variation of the energy gaps and local magnetic moments has been found, with no variation in the ordering of the occupied-bands. In our case the energy gaps increase by $\delta_{\text{Egap}} = 0.02$ eV for a positive strain of $\varepsilon = 0.02$, and reduces by $\delta_{\text{Egap}} = -0.02$ eV for a compressive strain $\varepsilon = -0.02$. These results are valid for all the studied GNR widths. Similar results are obtained for the local magnetic moments at the carbon edges, in all the cases the variation is on the order of $\pm 3\%$ for the same strain range studied.

4. Conclusions

In summary, the electronic and mechanical properties of stressed ZGNR were calculated using *ab initio* density functional theory. The proposed models allowed us to obtain the corresponding Young's modulus, shear modulus and Poisson's ratio for ZGNR with different widths. In all the cases the GNR present higher constants than graphene, but they approximate to this value when the GNR width is increased. This effect could be explained in terms of the hardness of the C–C bonds positioned at the edges of the GNR, due to the observed geometrical reconstruction. This property could lead to important consequences regarding the structure of the edge of this nanostructure, because chemical substitution, the appearance of defects, and chemical doping could soften or stiffen the edges. All these possibilities could lead to an important variation of the mechanical properties of GNR, in particular for the case of shorter GNR of low-dimensional systems. It would be interesting to simulate the presence of strong donating and strong acceptor groups as functional groups substituting the presence of the single H atoms. Regarding the mechanical properties, a linear dependency of stress upon strain has been observed in the region from $\varepsilon = -0.02$ to $+0.02$. A nonlinear dependence is found for higher strain. The electronic structure features are not sensitive to strain in this linear elastic regime, opening up the promise for the use of carbon nanostructures in nano-electronic devices in the near future.

Acknowledgments

The authors thank the PEDECIBA-Química and CSIC-Uruguayan organizations for their financial support.

References

[1] Son Y-W, Cohen M L and Louie S G 2006 *Nature* **444** 347
[2] Son Y-W, Cohen M L and Louie S G 2006 *Phys. Rev. Lett.* **97** 216803
[3] Campos-Delgado J, Romo-Herrera J M, Jia X, Cullen D A, Muramatsu H, Kim Y A, Hayashi T, Ren Z, Smith D J, Okuno Y, Ohba T, Kanoh H, Kaneko K, Endo M, Terrones H, Dresselhaus M S and Terrones M 2008 *Nano Lett.* **8** 2773
[4] Lee C, Wei X, Kysar J W and Hone J 2008 *Science* **321** 385
[5] Bekyarova E, Itkis M E, Ramesh P, Berger C, Sprinkle M, de Heer W A and Haddon R C 2009 *J. Am. Chem. Soc.* **131** 1336
[6] Denis P A, Faccio R and Mombrú A W 2009 *ChemPhysChem* **10** 715
[7] Ni Z H, Yu T, Lu Y H, Wang Y Y, Feng Y P and Shen Z X 2009 *ACS Nano* **3** 483
[8] Pereira V M, Castro Neto A H and Pereset N M R 2008 arXiv:0811.4396
[9] Braga S F and Galvão D S 2006 *Chem. Phys. Lett.* **419** 394
[10] Coluci V R, Dantas S O, Jorio A and Galvão D S 2007 *Phys. Rev.* B **75** 075417
[11] Coluci V R, Pugno N M, Dantas S O, Galvão D S and Jorio A 2007 *Nanotechnology* **18** 335702
[12] Caetano E W S, Freire V N, dos Santos S G, Galvão D S and Sato F 2008 *J. Chem. Phys.* **128** 164719
[13] Sun L, Li Q, Ren H, Su H, Shi Q W and Yang J 2008 *J. Chem. Phys.* **129** 074704
[14] Xu Z 2007 arXiv:0709.0992 [cond-mat]
[15] Su W S, Wu B R and Leung T C 2008 arXiv:0810.4582 [cond-mat]
[16] Blakslee O L 1970 *J. Appl. Phys.* **41** 3373
[17] Kudin K N, Scuseria G E and Yakobson B I 2001 *Phys. Rev.* B **64** 235406
[18] Van Lier G, Van Alsenoy C, Van Doren V and Greelings P 2000 *Chem. Phys. Lett.* **326** 181
[19] Reddy C D, Rajendran S and Liew K M 2006 *Nanotechnology* **17** 864–70
[20] Arroyo M and Belytschko T 2004 *Phys. Rev.* B **69** 115415
[21] Zhang P, Jiang H, Huang Y, Geubelle P H and Hwang K C 2002 *Int. J. Solids Struct.* **39** 3893
[22] Friesecke G and Theil F 2002 *J. Nonlinear Sci.* **12** 445
[23] Lu J P 1997 *Phys. Rev. Lett.* **79** 1297
[24] Reddy C D, Rajendran S and Liew K M 2005 *Int. J. Nanosci.* **4** 631
[25] Shen L and Li J 2004 *Phys. Rev.* B **69** 045414
[26] Yu M F, Files B S, Arepalli S and Ruoff R S 2000 *Phys. Rev. Lett.* **84** 5552
[27] Sammalkorpi M, Krasheninnikov A, Kuronen A, Nordlund K and Kaski K 2004 *Phys. Rev.* B **70** 245416
[28] Yoon J, Ru C Q and Mioduchowski A 2005 *Trans. ASME, J. Appl. Mech.* **72** 10
[29] Wu Y, Huang M, Wang F, Henry Huang X M, Rosenblatt S, Huang L, Yan H, O'Brien S P, H James and Heinz T F 2008 *Nano Lett.* **8** 4158–61
[30] Bogár F, Mintmire J W, Bartha F, Mezo T and Van Alsenoy C 2005 *Phys. Rev.* B **72** 085452
[31] Palacio F and Makarova T (ed) 2005 *Carbon-Based Magnetism* (Amsterdam: Elsevier)
[32] Miyamoto Y, Nakada K and Fujita M 1999 *Phys. Rev.* B **59** 9859
[33] Pisani L, Chan J A, Montanari B and Harrison N M 2007 *Phys. Rev.* B **75** 064418
[34] Hohenberg P and Kohn W 1964 *Phys. Rev.* **136** B864
[35] Kohn W and Sham L J 1965 *Phys. Rev.* **140** A1133
[36] Faccio R, Pardo H, Denis P A, Yoshikawa Oreiras R, Araújo-Moreira F M, Verisimo-Alves M and Mombrú A W 2008 *Phys. Rev.* B **77** 035416
[37] Denis P A and Faccio R 2008 *Chem. Phys. Lett.* **460** 491
[38] Denis P A, Iribarne F and Faccio R 2009 *J. Chem. Phys.* **130** 194704
[39] Ordejón P, Artacho E and Soler J M 1996 *Phys. Rev.* B **53** R10441
[40] Sánchez-Portal D, Ordejón P, Artacho E and Soler J M 1997 *Int. J. Quantum Chem.* **65** 453
[41] Soler J M, Artacho E, Gale J D, García A, Junquera J, Ordejón P and Sánchez-Portal D 2002 *J. Phys.: Condens. Matter* **14** 2745
[42] Troullier N and Martins J L 1991 *Phys. Rev.* B **43** 1993
[43] Perdew J P, Burke K and Ernzerhof M 1996 *Phys. Rev. Lett.* **77** 3865
Perdew J P, Burke K and Ernzerhof M 1997 *Phys. Rev. Lett.* **78** 1396
[44] Press W H, Flannery B P, Teukolsky S A and Vetterling W T 1986 *New Numerical Recipes* (New York: Cambridge University Press)
[45] Monkhorst H J and Pack J D 1976 *Phys. Rev.* B **13** 5188
[46] Liu F, Ming P M and Li J 2007 *Phys. Rev.* B **76** 064120
[47] Khare R, Mielke S L, Paci J T, Zhang S, Ballarini R, Schatz G C and Belytschko T 2007 *Phys. Rev.* B **75** 075412
[48] Liu F, Ming P M and Li J 2007 *Phys. Rev.* B **76** 064120
[49] Sakhaee-Pour A 2009 *Solid State Commun.* **149** 91
[50] Li C and Chou T-W 2003 *Int. J. Solids Struct.* **40** 2487–99
[51] Tserpes K I and Papanikos P 2005 *Composites* B **36** 468–77